#6020

International Symposium on Room Air Convection and Ventilation Effectiveness
University of Tokyo, July 22 – 24, 1992

An Application of k-ε Turbulence Model to Predict How a Rectangular Obstacle with Heat Flux in a Slot-Ventilated Enclosure Affects Air Flow

Hong-Lim Choi	Hyeon-Tae, Kim
Associate Professor	Research Assistant
Dept. of Agric. Engr.	Dept. of Agric. Engr.
Gyeongsang Nat'l Univ.	Gyeongsang Nat'l Univ.
Chinju, Korea 660-701	Chinju, Korea 660-701

ABSTRACT

A modification of the TEACH-like computer program based on the k-ε turbulence transport was applied to the problem of predicting air mixing patterns and tempertaure distributions in a slot-ventilated experimental piggery with obstructions; a rectangular obstacle with heat flux and a solid wall separates the passage and the pig pens. Air flow patterns and temperature distributions were calculated for the entering air temperatures of 17℃ and 10℃, with and without the solid walls. Overall similarities in flow patterns and temperature profiles were confirmed between the calculated and the observed in Boon (1978). A clear discrepancy in the calculated air flow pattern with data for a flow configuration of Reynolds number of 3E+3 and Arichemes number of 8.95E-3 (horizontally entering air temperature was 10℃) was observed. Perhaps discrepancy originated from the insentivity of k-ε turbulence model to thermal buoyancy, or from improper management of experiment. Further study should be conducted to explore the cause

KEYWORD k-ε Turbulence Model, Velocities, Tempertaure Distribution, Air Flow Patterns, Slot-ventilated.

non-isothermal mean flow. The equations are expressed in the Body-Fitted Coordinate(BFC) system, discussed more in the Body-Fitted Coordinate system.

1) Continuity:

$$\frac{\partial}{\partial x}(\rho U)+\frac{\partial}{\partial x}(\rho V)=0 \tag{3}$$

2) U-Momentum Equation:

$$\frac{\partial}{\partial x}(\rho U^2)+\frac{\partial}{\partial y}(\rho UV)=-\frac{\partial P}{\partial x}+\frac{\partial}{\partial x}\left(\mu_{eff}\frac{\partial U}{\partial x}\right)+\frac{\partial}{\partial y}\left(\mu_{eff}\frac{\partial U}{\partial y}\right)+S_u \tag{4}$$

where, $S_u=\frac{\partial}{\partial x}\left(\mu_{eff}\frac{\partial U}{\partial x}\right)+\frac{\partial}{\partial y}\left(\mu_{eff}\frac{\partial U}{\partial y}\right)$

3) V-Momentum Equation:

$$\frac{\partial}{\partial x}(\rho UV)+\frac{\partial}{\partial y}(\rho V^2)=-\frac{\partial P}{\partial y}+\frac{\partial}{\partial x}\left(\mu_{eff}\frac{\partial V}{\partial x}\right)+\frac{\partial}{\partial y}\left(\mu_{eff}\frac{\partial V}{\partial y}\right)+\rho_r g\beta(T-T_r)+S_v \tag{5}$$

where, $S_v=\frac{\partial}{\partial x}\left(\mu_{eff}\frac{\partial V}{\partial x}\right)+\frac{\partial}{\partial y}\left(\mu_{eff}\frac{\partial V}{\partial y}\right)$

4) Energy Transport Equation:

$$\frac{\partial}{\partial x}(\rho Uh)+\frac{\partial}{\partial y}(\rho Vh)=\frac{\partial}{\partial x}\left(\gamma_{eff}\frac{\partial h}{\partial x}\right)+\frac{\partial}{\partial y}\left(\gamma_{eff}\frac{\partial h}{\partial y}\right)+S_h \tag{6}$$

where, S_h : source terms like heat flux

5) Turbulent kinetic energy equation (k-equation):

$$\frac{\partial}{\partial x}(\rho Uk)+\frac{\partial}{\partial y}(\rho Vk)=\frac{\partial}{\partial x}\left(\frac{\mu_{eff}}{\sigma_k}\frac{\partial k}{\partial x}\right)+\frac{\partial}{\partial y}\left(\frac{\mu_{eff}}{\sigma_k}\frac{\partial k}{\partial y}\right)+G-C_D\rho\varepsilon+G_B \tag{7}$$

where, $G=\mu_t\left[\left\{2\left(\frac{\partial U}{\partial x}\right)^2+\left(\frac{\partial U}{\partial x}\right)^2\right\}+\left(\frac{\partial U}{\partial y}+\frac{\partial V}{\partial x}\right)^2\right]$: $G_B=\beta g\left(\frac{\mu_t}{\sigma_t}\right)\frac{\partial\theta}{\partial y}$: $\theta=T-T_r$

6) Dissipation rate of Turbulent Kinetic Energy (ε-equation):

$$\frac{\partial}{\partial t}(\rho\varepsilon)+\frac{\partial}{\partial x}(\rho U\varepsilon)+\frac{\partial}{\partial y}(\rho V\varepsilon)=\frac{\partial}{\partial x}\left(\frac{\mu_{eff}}{\sigma_e}\frac{\partial\varepsilon}{\partial x}\right)+\frac{\partial}{\partial y}\left(\frac{\mu_{eff}}{\sigma_e}\frac{\partial\varepsilon}{\partial y}\right)+\frac{\varepsilon}{k}(C_1G-C_2\rho\varepsilon)+C_3\frac{\varepsilon}{k}G_B \tag{8}$$

<Table 1> Value of Constants in the Turbulence model

C_μ	C_D	C_1	C_2	C_3	σ_k	σ_e
0.09	1.0	1.44	1.92	1.0	1.0	1.3

III. Numerical Analysis

1. Grid Generation for Body-Fitted Coordinates

1) Equations

In general, grid generation is a mapping between a physical space and a computational space. The transformation is given by the functions

$$\xi = \xi\ (x, y) \quad (9a)$$

$$\eta = \eta\ (x, y) \quad (9b)$$

where ξ and η represent coordinates in the transformed computational plane in Fig. 1.
In this method employed in the grid generation program reported here, the generating functions are either Laplace equations or Poisson equations. Use of the Laplace equations yields

$$\xi_{xx} + \xi_{yy} = 0 \quad (10a)$$

$$\eta_{xx} + \eta_{yy} = 0 \quad (10b)$$

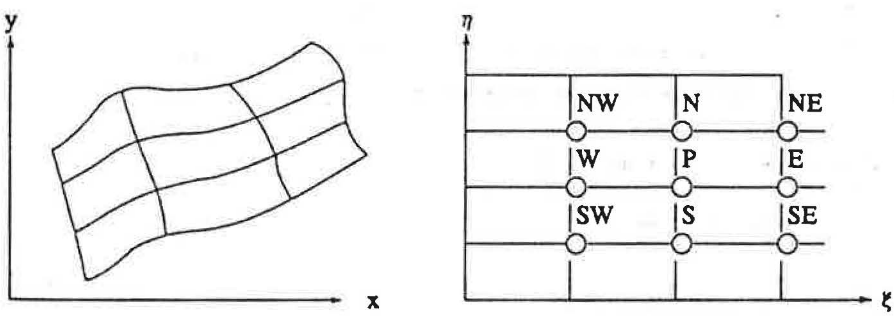

a. Physical Plane　　b. Computational Plane

<Fig. 1> Mapping from Physical Plane to Computational Plane

Solution of this set of equations will result in a grid system with maximum orthogonality of the grid lines, but the grid line spacing will be as unifrom as possible. There is no way to control the spacing of interior points. In order to cluster grid points or lines spacing, it is necessary to incorporate control functions (P,Q) into Eq. (11) and (12). This results in a Poisson equation for the transformation.

$$\xi_{xx} + \xi_{yy} = P\ (\xi, \eta) \quad (11a)$$

$$\eta_{xx} + \eta_{yy} = Q\ (\xi, \eta) \quad (11b)$$

2) Discretization of the Equations

The Laplace euqations (10a,b) can be transformed to the computatioal plane, resulting in two elliptic equations in the form

$$\alpha x_{\xi\xi} - 2\beta x_{\xi\eta} + \gamma x_{\eta\eta} = 0 \quad (12a)$$

$$\alpha y_{\xi\xi} - 2\beta y_{\xi\eta} + \gamma y_{\eta\eta} = 0 \quad (12b)$$

where, $\alpha = x_\eta^2 + y_\eta^2$; $\beta = x_\xi x_\eta + y_\xi y_\eta$; $\gamma = x_\xi^2 + y_\xi^2$ (12c)

3) Soution Procedure

Rearrangement of Eq.(10) for finite difference form of the x-equation yields xP at the grid locations shown in Fig.1b.

$$x_P = \frac{a_N x_N + a_S x_S + a_E x_E + a_W x_W + S_U}{a_N + a_S + a_E + a_W - S_P} \quad (13a)$$

where, $S_U = B/2(x_{NE} - x_{NW} + x_{SW} - x_{SE})$ (13b)

$S_P = 0$ (13c)

The convergence criterion for the overall solution procedure consists of a user-specified reduction in the sum of the residuals of the euqations. At the iteration a residual is calculated at each point according to:

$$\varepsilon = \frac{a_N x_N + a_S x_S + a_E x_E + a_W x_W + S_U}{a_N + a_S + a_E + a_W - S_P} - x_P \quad (14)$$

2. Formulation of Discretized Equations

Eq. (3)~(8) can be discribed by the differential equations of the form for single phase flow. $\phi = 1$ yields the continuity equation.

$$\frac{\partial}{\partial t}(\rho\,\phi) + \nabla(\rho\,\phi\,V) - \nabla(\Gamma_s \nabla\phi) = S_s \quad (15)$$

The values of the flow variables at each cell and for each time-step are the sought-for outcome of the compuatation. Fig.1a is the control voulme for scalar and (b) for velocities. The code uses the staggered-grid arrangement (Fig. 1b), in which the location of the velocity nodes is displaced with respect to the location of the node used for other scalar variables, and located or

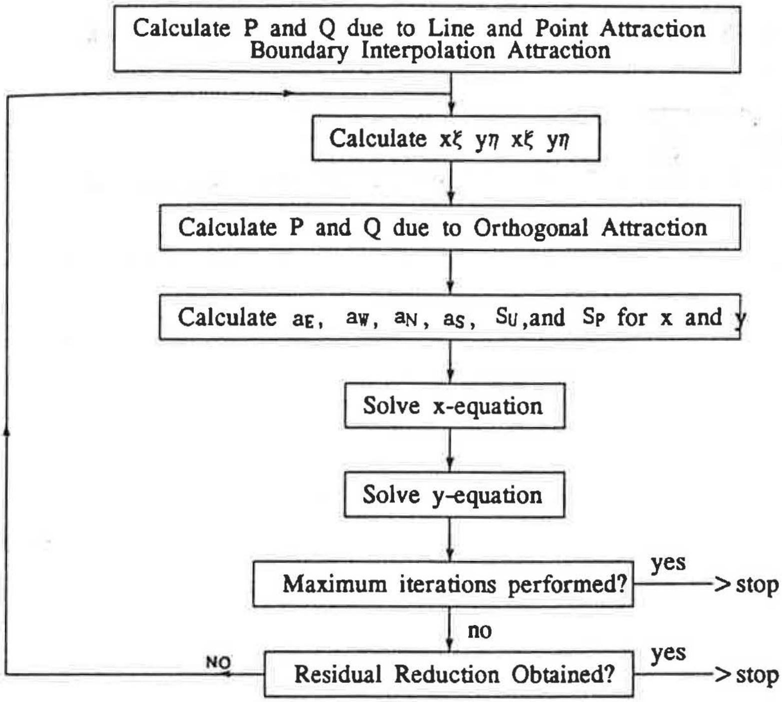

<Fig. 2> Solution Procedure

the cell faces. The benefits of this arrangement are that each velocity component is driven by two adjacent pressures and the value of the velocity is avaiable, without interpolation, at the cell face, where it will be needed to computer the convection fluxes into cell.

The results of the intergration process can be grouped into an equation of the form:

$$a_P\phi_P = a_N\phi_N + a_S\phi_S + a_E\phi_E + a_W\phi_W + a_T\phi_T + b \qquad (16)$$

where, $a_E = \rho A_E [- U_e] + D_E$, for example.

$$a_T = (V_P/\triangle t)\rho_T$$

$$b = V_P C\phi_P V\phi_P$$

Eq.(16) can be rewritten for ϕ_P as:

$$\phi_P = \frac{a_E\phi_E + a_W\phi_W + a_N\phi_N + a_S\phi_S + a_T\phi_T + b}{a_E + a_W + a_N + a_S + a_T + a_P} \qquad (17)$$

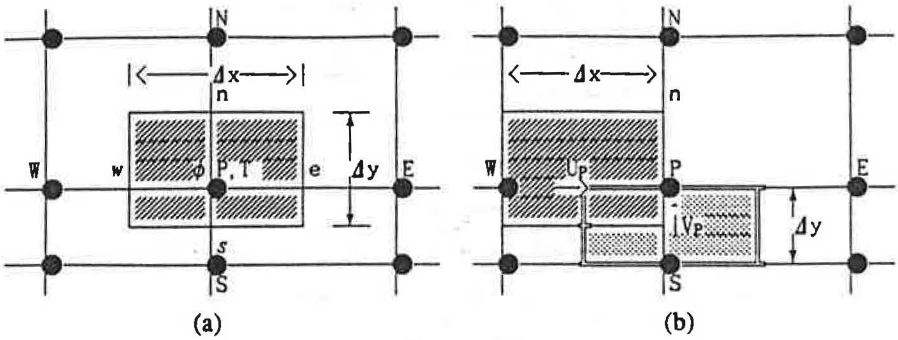

<Fig. 3> Two dimensional calculation domain for (a) scalar (b) U-velocity(▨), V-velocity(░) in computational plane.

3. Linerization of source term

When the source term S depends on ϕ, the dependence can be linearized by Eq.(18). This is done because our nominally linear framework would allow only a formally linear dependence, and the incorporation of linear dependence is better than treating S as a constant.

$$S = S_C + S_P \phi_P \tag{18}$$

S_C includes in b, and $-S_P$ in ap in Eq.(16).

4. SIMPLE-like Algorithm

The solution algorithm is a marching one, that sweeps the domain in a slab-by-slab fashion. A slab is an X-Y plane of cells, and contains NX * NY cells. The code has three levels of iteration. The iternation level 1 in Fig. 2 the NX * NY system of equations for a variable ϕ at each slab, using either a generalized 2D version of the well-known Tri-Diagonal Matrix Algorithm (TDMA) or a Jacobi point by point procedure. The iteration level 2 has to blend together the changes effected for each variable separately. The pressure/velocity linkage has also to be dealt with this level. The pressure field has to be such that the velocities resulting from the momentum equations verify the continuity equation.

The iteration level 3 repeatly solve the equations for all variables including pressure correction updating the corrections between them. In the slab by slab procedure, the off-slab values are assumed known, whereas they are not. As a consequence, the solution for the current slab is not the final one, and the solution procedure has to sweep all the slab in the domain several level.

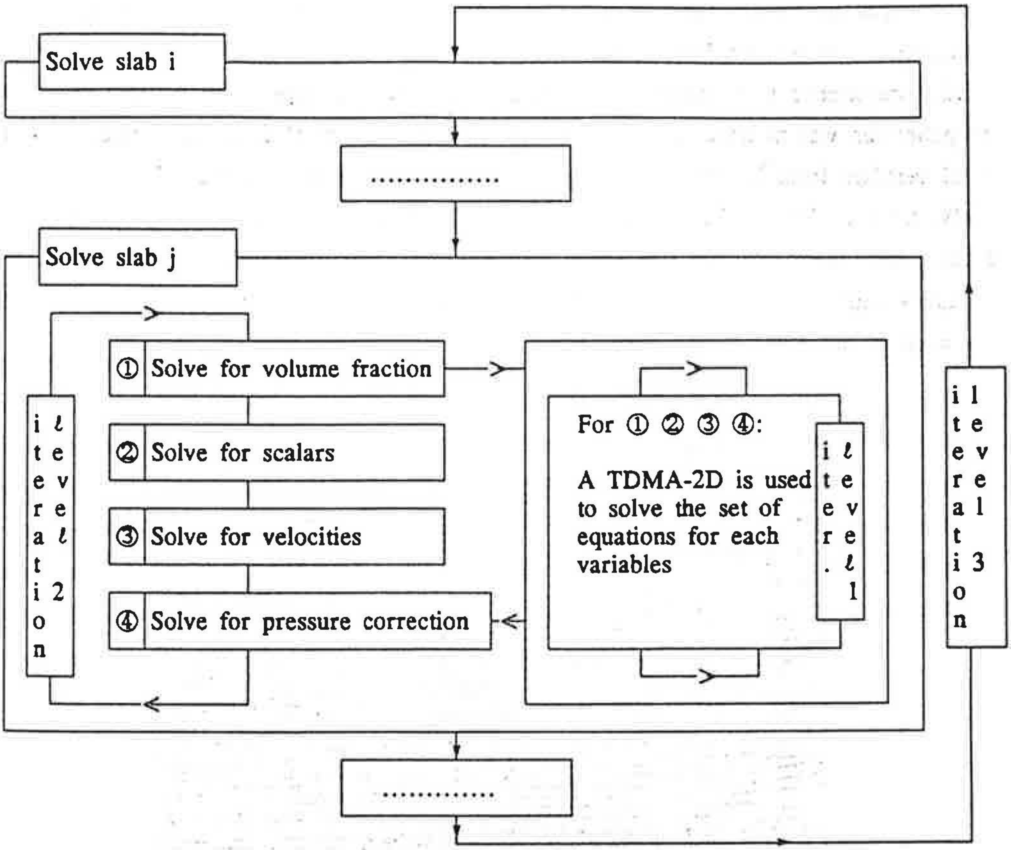

<Fig. 4> Solution Algorithm for two dimensional discretized equations.

VI. Result and Discussion

Air flow patterns in <Fig. 6a> ~ <Fig. 10a> were visualized by Boon(1978), using liquid film bubbles in the flow. <Fig. 6a> ~ <Fig. 10a> were used to examine the ability of the simulation model applied in predicting a realistic air flow.

1. Experimetal Procedure

The full-scale section of a livestock building used for calculation geometry, <Fig. 5> ,in this work was described in detail in Boon(1978). The section was 7.80 m wide representing a typical span which may accomodate two pig pens and three passages. It was arranged with solid walls, 1.05 m high, to form a feeding passage at each side and with a central wall to form two pens. The outlay of the experimental livestock building is shown in <Fig. 6> with the presence, and <Fig. 7> with the absence of solid walls. The depth of the section represented the length of one pen and the height was 1.87 m to the eaves and 2.43 m to the ridge. An insulated shell connected to an air conditioner and enclosing the side walls and roof allowed the temperature outside the section to be controlled. Ventilating air was exhausted from the shell by a 0.457m propeller fan was mounted 0.45 m above the ceiling in a vertial duct. Heat released from the stock resulted from 26 large white pigs, 13 in each pen, generating heat 170 W/m^2 for 10℃, 130W/m^2 for 17℃. The air inlet was a 0.041 m wide slit, the full length of the building section, near the top of each side wall 1.70 m from the floor. Approximately 0.52 m^3/s for inlet air temperature of 17℃ and 0.16m^3/s for 10℃. The outlet was 0.52 m^2 aperture in the center of the apex of the roof.

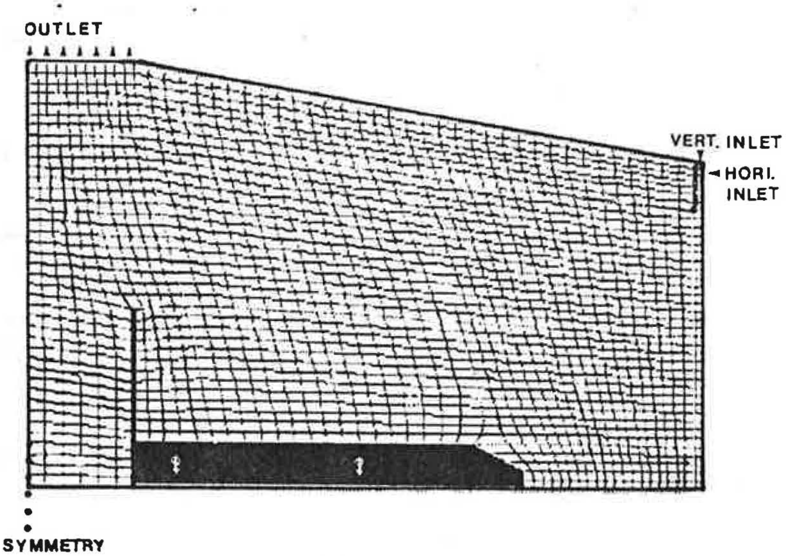

<Fig. 5> Calculation domain with Body-Fitted Coordinate system

2. Air Flow Patterns

1) The Effect of Obstruction

The inlet air jet enters horizontally in flow configurations of <Fig. 6> and <Fig. 7> with the entering air temperature of 17℃ (equivalent to Arichimedes number of 1.25E-4) and Reynolds number of 10,000. The only difference in the flow configurations is the presence of physical obstruction. Overall similarities were perceived between the calculated and the observed air flow in <Fig. 6> and <Fig. 7>. No distinct difference of air motion is observed in <Fig. 6a> and in <Fig. 7a> either with or without internal obstacles. There is, however, some difference in the size of a primary recirculation flow. Boon's observation do not show the details of air motion and the magnitude of air velocities, but calculations in this work, reveal such details <Fig. 6b> and <Fig. 7b>. The more detailed air motion in this work provides additional information.

The calculated air flow of <Fig. 6b> with the presence of an obstacle shows primary recirculation in the center of the space; it rotates counterclockwise and is squeezed due to the solid wall. A seconadry recirculation flow is observed between the symmertric line and the internal solid wall, which separates the passage and the pig pen. Initially a free air jet in <Fig. 6b> deflects upwards and attaches to the ceiling due to Coanda effect. The reattached flow becomes a wall jet and continues to move along the ceiling. The solid wall creates a dominating adverse pressure gradient, which leads to flow separartion. A weak eddy is also observed in the lower right corner of <Fig. 6b>.

The physical obstructions in <Fig.6> modifies air flow significantly. They deflect air flow and lead to flow separations by creating adverse pressure gradient, and dissipates the turbulent kinetic energy of the air flow. In most cases, physical obstructions adversely effect to air flow. However, they purposefully were utilized to redirect or to decelerate air flow. As shown in <Fig. 6b>, air velocities are relatively smaller, compared to those of <Fig. 7b>. In paricular, the air velocities approaches zero at the height of animals while those in other regions has larger velocities. Except in cold winter, it is desirable to have higher air velocities to maintain proper indoor thermal and chemical environments.

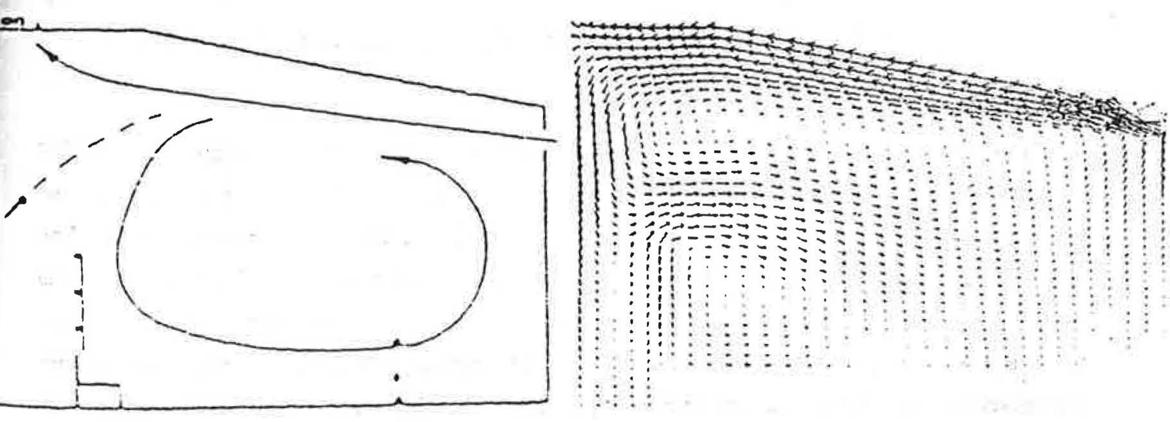

(a) (b)

<Fig. 6> a) the observation by Boon(1978) b) the calculated flow patterns

Short-circuiting phenomenum is observed in the flow configuration of <Fig. 6> and <Fig, 7>. Much of the entering air flow through the slot inlet at eave are exhaused by the fan at the ridge. A recirculating air forms a primary flow with lower velocity, so with lower momentum, rotates counterclockwise, and it again separates at the top of the internal solid wall. Some of them are entrained by the inlet air jet, and the rest forms the secondary eddy rotates clockwise in the region between the internal solid wall and the inlet wall. Basically, air flow with less momentum has less ability in diluting contaminants. Excessive harmful gases or dust may accumlulate on the pigs or on the floor since the overall velocity is much smaller in the flow field.

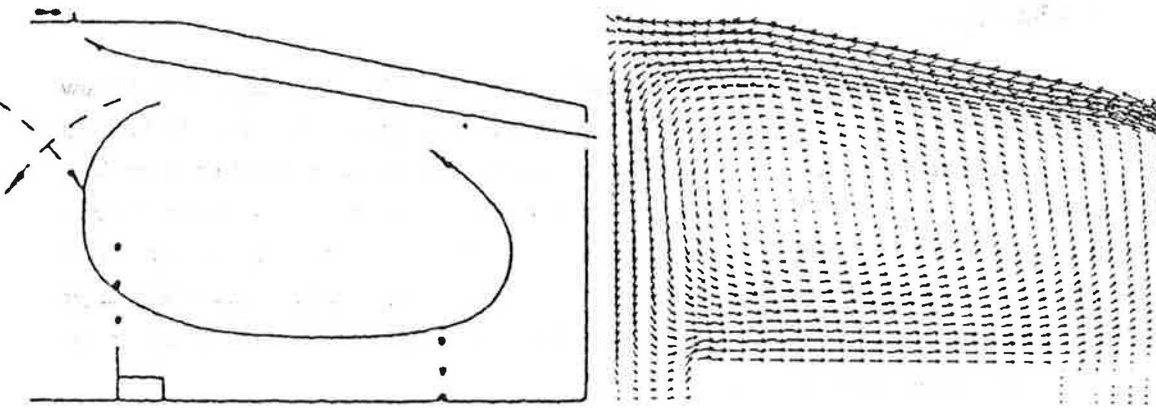

(a) (b)

<Fig. 7> a) the observed by Boon(1978) b) the calculated flow patterns

2. The Effect of Ambient Temperature

To see the effect of thermal buoyancy force on air flow, the entering air temperature of 10℃ was applied to the flow geometry of <Fig. 8> with heat flux of 170 W/m^2, released from real pigs at floor (equivalent to Archimedes number of 8.95E-3) and Reynolds number of 3,000. The calculated air flow in <Fig. 8b> moves forwards, and falls down in the middle of the space and rotates clockwise. This may indicate that that buoyancy force overcomes inertia force. However, the observed air flow in <Fig. 8a> falls down immediately after entering, and rotates counter-clockwise. Perhaps discrepancy of the observed in <Fig. 8a> and the calculated air flow in <Fig. 8b> originated from the insensitivity of the k-ε turbulence model itself to buoyancy, based on experience, or from improper management of experiment. Since the flow is a fully-developed and a turbulent flow, the inertia force may overcome buoyancy force to some distance from the inlet.

If such a ventilation system is adapted in cold winter, it may create a problem. When a very cold air jet drops on the head of animals, it causes a chilly draft to the animals. It is recommended to direct air flow downward so that the cold jet gets warmer along the inside wall.

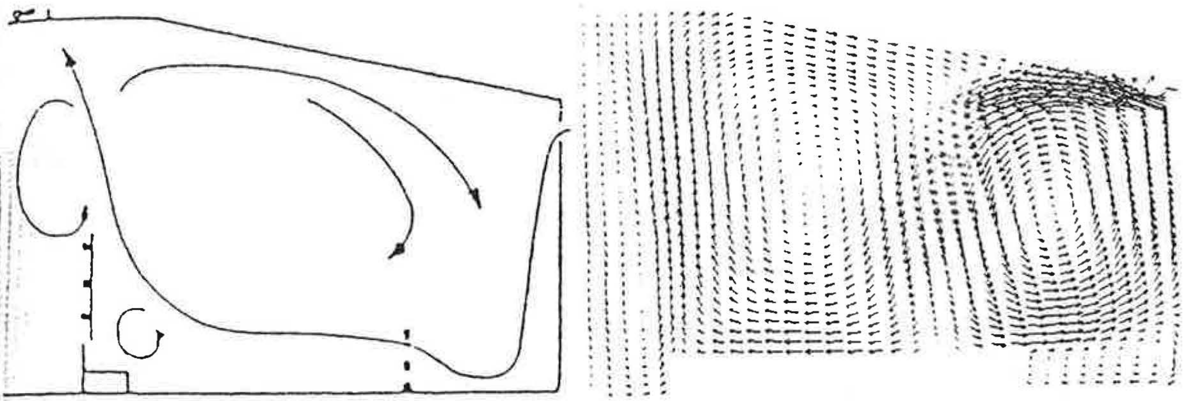

(a) (b)

<Fig. 8> a) the observed by Boon(1978) b) the calculated flow patterns

3. The Effect of Direction of Inlet Air Jet

A typical ventilation system in a cold winter directs entering air jet downwards, and moves along the wall so the air gets warmer to avoid draft to animals. <Fig. 9b> shows a flow pattern for the vertical inlet air flow with temerature of 17℃ and Reynolds number of 10,000. It is expected the inertia force of the flow is predominant. As shown in <Fig. 9b>, A strong air jet rotates clockwisely and impinges an obstacles which prevents air flow from diffusing to the left-half of the space. A primary recirculation flow rotates clockwise and attaches to the roof and separates. Some of them forms a secondary recirculation flow in the left-half region of the space, and much is entrained by an inlet air jet, due to strong adverse pressure gradient. Small eddies can be observed in the upper-left corner of the obstacle, similar with the observed in <Fig. 9a>, and in the lower region between the symmetric axis and the solid wall. A major concern in <Fig. 9b> is the discrepancy of the magnitude of air velocities between the right-half and the left-half is so large that much of the secondary flow in the left-half region of the space is exhaused to outlet. The left-half region can be considered to as a stagnant region. The ventilation system can not dilute contaminants due to incomplete air mixing. The size of recirculation flows in <Fig. 9b> is much different from those in <Fig. 9a>. This may be caused by improper reflection of real pigs beavior laying at the floor to boundary condition in the calculation, which is referred to as an obstacle; sometime pigs in the pen move around, or by the insenstivity of the k-ε turbulence model to buoyancy.

The observed air flow for <Fig. 9> with Ar= 2.64E-4 and Re =1E+4, and the air flow for <Fig. 10> with Ar=8.95E-2 and Re=3E+3 are basically same as the calculated.

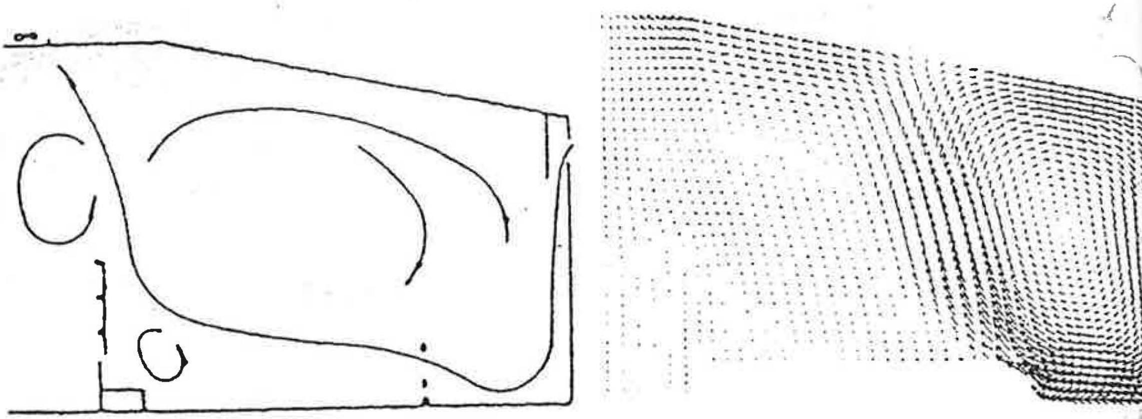

(a) (b)

<Fig. 9> a) the observed by Boon(1978) b) the calculated flow patterns

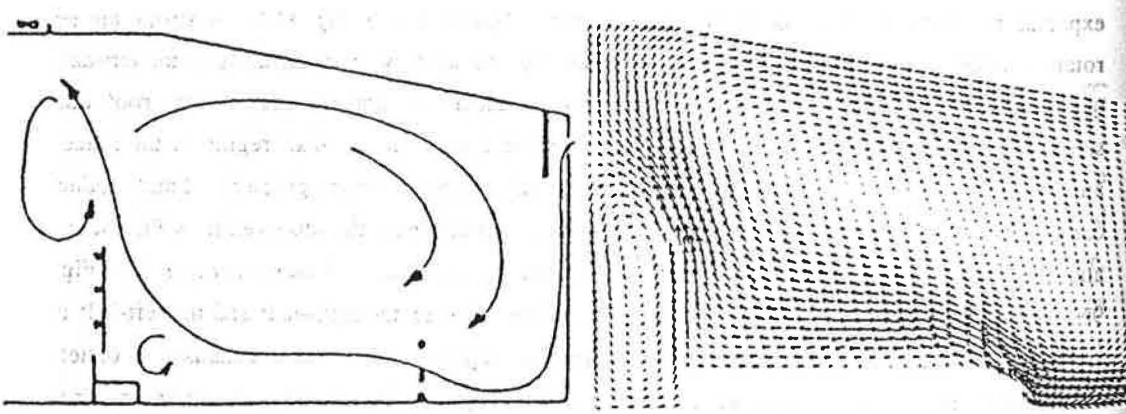

(a) (b)

<Fig. 10> a) the observed by Boon(1978) b) the calculated flow patterns

VI. Conclusion

The TEACH-like program, which uses the k-ε turbulence model, was applied to a ventilated air space having obstructions; 26 real pigs with heat flux of 130 W/m^2 for inlet temperature of 17 ℃ and Reynolds number of 1E+4, and 170W/m^2 for 10℃ and Re of 3E+3. Results were compared to experimental data and the following conclusions were drawn.

1. It is possible to predict, with reasonable accuarcy, overall flow patterns and temperature distribution in a ventilated space, represneting a typical livestock building having phyical obstructions, by solving discretized conservation equations and using the standard k-ε model.

2. Obstructions in a ventilated space significantly modifies air flow and/or creates dead regions. The obstacle like the real pigs in the geometric configuration of <Fig. 9b> dissipates most kinetic energy of the air jet due to impingement, which eventually leads to imcomplete mixing due to lack of momentum of the flow. It should avoid the obstruction in the route of the inlet air jet flow since the inlet jet governs the whole flow field.

3. The ventlation system, having inlets at the eaves and outlet at ridge leads air flow short-circuited. Such a system lowers the effectiveness so that it is easy to create the dead regions.

4. The buoyancy force orginated from the temperature difference between the entering air and the heat flux from the real pigs moves air flow upwards. Heat accumulation can be observed in the stagnant region created by obstructions.

5. It is prerequiste to simulate air flow and temperature distributions in a ventilated space for design purpose to evaluate the efficiency of the ventilation system to be condstructed.

<Symbols>

a's : coefficents in finite-domain equation in Eq.(16)
b : source term of ϕ in Eq.(16)
U : Horizontal mean velocity
V : Vertical mean velocity
k : turbulent kinetic energy
ε : the rate of dissipation of turbulent kinetic energy
h : enthalpy
S : a source term in Eq.(18)
ρ : density
α : upwinding-scheme control parameter
β : coefficient of gas expansion
$C\mu$: coefficient
μeff : effective turbulent viscosity
μ : laminar viscodity
σ : laminar Prandtl (Pr) number
σt : turbulent Prandtl number
ϕ : varaibles in question in Eq.(15)

<Subscripts>

P : grid node loaction at the center of the domain or Pressure
N : grid node at north
S : grid node at south
E : grid node at east
W : grid node at west
T : time step node
D : diffusion
l : laminar
t : turbulent

Reference

Albright L.D. 1984. Building Environmental Control, AE682 Lecture Notebook, Conrell University, Ithaca, NY.

Barber E.M. 1981. Scale-model study of incomplete mixing in a ventilated air space. Unpublished Ph.D. Thesis, University of Guelph.

Boon, C.R. 1978. Airflow patterns and temperature distribution in an experimental piggery. JAER 23(2):129～139.

Boon, C.R. 1984. The control of Climate Environment for finishing pigs using lower critical temperature. JAER 29:295～303.

Carpenter, G.A.,L.J. Mousley & J.M.Randall. 1972. Ventilation investigation using a section of a livestock building and air flow visualization by bubbles. JAER 17(4):323～331.

Carpenter, G.A.,L.J. Mousley. 1978. Resistance to airflow of materials used in ventilating livestock buildings. JAER 23:441～451.

Hellickson M.A. and J.N. Walker(editors). 1983. Ventilation of Agricultural Structures. ASAE Monograph No.6. St.Joseph, MI.

Hong-Lim Choi. 1989. Ventilation of Agricultural Structures. Daegwang Pub.

Hong-Lim Choi & Won-Myung, Suh. 1988. Determination of Environmental Parameters for Agricultural Production Structures. J. Inst. Agr. Res. Util. Gyeongsang Nat'l University 22(2):221.

Hong-Lim Choi, Hyeon-Tae Kim, & Woo-Joong, Kim. 1991. Development of New Conceptual Ventilation Graphs for Mechanically Ventilated Livestock Buildings. Trans. of KSAE 33(3):91～100.

Hong-Lim Choi, L.D. Albright, M.B.Timmons & Z.Warhaft. 1988. An Application of the k-ε turbulence model to predict air distribution in a slot-ventilated enclosure. Transaction. ASAE 31(6):1804～1814.

Hong-Lim Choi, L.D. Albright & M.B.Timmons. 1990. An Application of the k-ε turbulence model to predict how a rectangular opbstacle in a slot-ventilated enclosure affects air flow. Transaction. ASAE 33(1):274～281.

Patankar, P.V. 1980. Numerical Heat Transfer and Fluid Flow. McGraw-Hill Book Company. NY.

Pattie,D.R. & W.R. Milne. 1966. Ventilation air flow patterns by using of models. Transaction ASAE 9(5):646～649.

Randall, J.M. 1975. The prediction of air flow patterns in a livestock building. JAER 20(2):199～215.

Randall, J.M & V.A. Battams. 1976. The observed influence of surface obstructions on the airflow pattern within livestock building. JAER 21(1):33～39.

Randall, J.M. 1979. The stability criteria for airflow patterns in livestock buildings. JAER 24:361～374.

Rodi, W. 1984. Turbulence Models and Their Applications in Hydraulics-A State of the Art Review.(1st ed.). International Association for Hydraulic Research, Delft.

Tennekes, H. and J.L. Lumley. 1972. A First Course in Turbulence. MIT Press,Cambridge, MA.

Timmons, M.B. 1979. Experimental and numerical study of air movement in slot-ventilated enclosures. Unpublished Ph.D. Thesis, Cornell University.

Timmons, M.B. 1984. Internal air velocity as affected by the size and location of continuous inlet slots. Transaction ASAE 27(5):1514～1517.